Effect of Ionospheric Variability on the Electron Energy Spectrum produced from Incoherent Scatter Radar Measurements

Oliver Stalder, Björn Gustavsson

April 18, 2023

Abstract

The ionospheric composition is modeled for relevant major and minor species at 80 - 150 km during auroral precipitation. The model is combined with the ElSpec algorithm [6] to produce the differential energy spectrum from incoherent scatter radar measurements. The impact of ionospheric variability on the inversion is shown. We find up to ... % deviations in the differential energy spectrum and up to ...% deviation in field aligned current compared to a constant ionosphere model.

1 Introduction

Ion density variations in the ionosphere can significantly influence the recombination time of electrons. This has direct influence on inversion techniques that use electron density profiles to infer differential energy spectra of electrons precipitating during aurora.
Electron density inversion makes use the electron continuity equation:

$$\frac{dn_e}{dt} = q_e - \alpha_{eff} n_e^2 + \nabla \cdot (n_e \boldsymbol{v_e}) \tag{1.1}$$

with n_e being the electron density, q_e the production and α_{eff} the effective recombination rate. The convective term $\nabla \cdot (n_e \boldsymbol{v_e})$ is usually neglected due to the lack of information on the velocity vector. Transport and ionization of electrons precipitating in the ionosphere are governed by a set of linear differential equations, allowing to formulate the production height profile as a matrix product with a discretized differential energy flux ϕ:

$$q_e = A\phi \tag{1.2}$$

with A representing the production rates at discrete energies and altitudes [2, 5]. If the effective recombination rate is assumed constant, the problem is largely independent from ion densities. However, the recombination rate depends on the ion densities:

$$\alpha_{eff} = \alpha_{\mathrm{NO^+},e} \frac{n_{\mathrm{NO^+}}}{n_e} + \alpha_{\mathrm{O_2^+},e} \frac{n_{\mathrm{O_2^+}}}{n_e} \tag{1.3}$$

The ion densities are again given by their continuity equations. It has been shown that the ionospheric composition varies greatly during auroral precipitation [3] and it is assumed to have a considerable effect on electron inversion techniques [6]. This is the first study, to the author's knowledge, that takes the full dynamic variability into account by accurately modeling the relevant ion and minor species densities.

2 Method

2.1 Ion Chemistry

To model the ionospheric composition in response to the precipitation, the coupled continuity equations for minor neutral and in species (H, H+, N(4S), N(2D), N+, N2+, NO, NO+, O(1D), O(1S),

O+(4S), O2+) are integrated in time:

$$\frac{dn_k}{dt} = q_k - l_k \tag{2.1}$$

$$n_k(t) = n_k(t_0) + \int_{t_0}^{t} \frac{dn_k}{dt} dt \tag{2.2}$$

where production and loss terms are of the form $q_k = \sum_{i,j\to k} \alpha_{ij} n_i n_j$ and $l_k = -\sum_{i,k} \alpha_{ik} n_i n_k$, summed over all relevant reactions. Table 2.1 shows the reactions and reaction rates taken into account. In addition, ionization of major neutral species from electron precipitation is accounted for [4]:

$$q_{A,O^+} = q_e \frac{0.56\, n_O}{0.92\, n_{N_2} + n_{O_2} + 0.56\, n_O} \tag{2.3}$$

$$q_{A,N_2^+} = q_e \frac{0.92\, n_{N_2}}{0.92\, n_{N_2} + n_{O_2} + 0.56\, n_O} \tag{2.4}$$

$$q_{A,O_2^+} = q_e \frac{n_{O_2}}{0.92\, n_{N_2} + n_{O_2} + 0.56\, n_O} \tag{2.5}$$

2.2 Electron Profile inversion

Inverting the electron density height profiles to differential energy spectra is performed with the ElSPec algorithm [6], extended by a robust statistics implementation [B. Gustavsson, unpublished]. The implementation of ElSPec used requires the entire data set to be processed at once. Therefore, instead of combining the ion chemistry model at each timestep with ElSpec, an iterative approach is adopted: The ElSpec algorithm is started with an assumed ionospheric composition, producing an electron production model q_e in altitude and time. This is then used in the ion chemistry model to calculate the evolution of ionospheric composition, and given as an input into the next iteration of ElSpec. Over few iterations, the ionospheric composition is converging to negligibly small deviations in between iterations.

2.3 Initial Composition

The International Reference Ionosphere (IRI) [1] is used as a model for the initial ion composition. As the IRI model cannot account for auroral precipitation and the induced changes in composition, a 30 minute time window is added to the start of the data set. During that time, the ionospheric chemistry model is run, assuming a constant electron and ion production rate, according to that of the first data point. The model ionosphere thereby reaches an equilibrium state. Figure 2.1 shows how NO^+ density at 98 km altitude reaches an equilibrium state.
Lastly, to suppress oscillations between iterations, the deviations in densities are damped by a factor of 2.

3 Results

A data set from the 12th of December 2006, recorded with the EISCAT UHF radar in Tromsø is analyzed. First, the convergence of this approach is tested. Figure 3.1 shows the mean relative deviation in the effective recombination rate between iterations, and the maximum relative deviation. There is a clear convergence until the 10th iteration.

Figure 3.4 shows a comparison between the inversion results obtained with a non-variable and variable ionosphere. - FAC modulation - slight differences in energy spectra, effects on electron profile

Reaction	Rate $[m^{-3}s^{-1}]$	Branching ratio
$O_2^+ + e^- \longrightarrow O(1D) + O(1S) + O$	$\alpha_1 = 1.9 \times 10^{-13} \, (T_e/300)^{-0.50}$	1.20, 0.10, 0.70
$N_2^+ + e^- \longrightarrow N(2D) + N(4S)$	$\alpha_2 = 1.8 \times 10^{-13} \, (T_e/300)^{-0.39}$	1.90, 0.10
$NO^+ + e^- \longrightarrow O + N(2D) + N(4S)$	$\alpha_3 = 4.2 \times 10^{-13} \, (T_e/300)^{-0.85}$	1.00, 0.78, 0.22
$N(4S) + O_2 \longrightarrow NO + O$	$\beta_1 = 4.4 \times 10^{-18} \, \exp(-3220/T_n)$	
$N(2D) + O_2 \longrightarrow NO + O(1D) + O$	$\beta_2 = 5.3 \times 10^{-18}$	1.00, 0.10, 0.90
$N(4S) + NO \longrightarrow N_2 + O$	$\beta_4 = 1.5 \times 10^{-18} \, T_n^{0.50}$	
$N(2D) + O \longrightarrow N(4S) + O$	$\beta_5 = 2.0 \times 10^{-18}$	
$N(2D) + e^- \longrightarrow N(4S) + e^-$	$\beta_6 = 5.5 \times 10^{-16} \, (T_e/300)^{0.5}$	
$N(2D) + NO \longrightarrow N_2 + O$	$\beta_7 = 7.0 \times 10^{-17}$	
$O^+(4S) + N_2 \longrightarrow NO^+ + N(4S)$	$\gamma_1 = \begin{cases} 5 \times 10^{-19} & T \leq 1000 \\ 4.5 \times 10^{-20} \, (T/300)^2 & T > 1000 \end{cases}$	
$O^+(4S) + O_2 \longrightarrow O_2^+ + O$	$\gamma_2 = 2.0 \times 10^{-17} \, (T_r/300)^{-0.40}$	
$N_2^+ + O \longrightarrow NO^+ + N(2D)$	$\gamma_4 = 1.4 \times 10^{-16} \, (T_r/300)^{-0.44}$	
$N_2^+ + O_2 \longrightarrow O_2^+ + N_2$	$\gamma_5 = 5.0 \times 10^{-17} \, (T_r/300)^{-0.80}$	
$O_2^+ + N_2 \longrightarrow NO^+ + NO$	$\gamma_8 = 5.0 \times 10^{-22}$	
$N^+ + O_2 \longrightarrow NO^+ + O + O(1D)$	$\gamma_{10} = 2.6 \times 10^{-16}$	1.00, 0.30, 0.70
$N^+ + O_2 \longrightarrow O_2^+ + N(4S)$	$\gamma_{11} = 1.1 \times 10^{-16}$	
$O^+(4S) + H \longrightarrow H^+ + O$	$\gamma_{12} = 6.0 \times 10^{-16}$	
$O_2^+ + NO \longrightarrow NO^+ + O_2$	$\gamma_{15} = 4.4 \times 10^{-16}$	
$O_2^+ + N(4S) \longrightarrow NO^+ + O$	$\gamma_{16} = 1.8 \times 10^{-16}$	
$O_2^+ + N(2D) \longrightarrow N^+ + O_2$	$\gamma_{17} = 2.5 \times 10^{-16}$	
$N_2^+ + NO \longrightarrow NO^+ + N_2$	$\gamma_{18} = 3.3 \times 10^{-16}$	
$N_2^+ + O \longrightarrow O^+(4S) + N_2$	$\gamma_{19} = 1.4 \times 10^{-16} \, (T_r/300)^{-0.44}$	
$H^+ + O \longrightarrow O^+(4S) + H$	$\gamma_{20} = (8/9)\gamma_{12}\sqrt{\frac{Ti+T_n/4}{T_n+Ti/16}}$	
$O^+(4S) + NO \longrightarrow NO^+ + O$	$\gamma_{21} = 8.0 \times 10^{-19}$	
$O^+(4S) + N(2D) \longrightarrow N^+ + O$	$\gamma_{26} = 1.3 \times 10^{-16}$	
$N^+ + O_2 \longrightarrow O^+(4S) + NO$	$\gamma_{27} = 3.0 \times 10^{-17}$	
$N^+ + O \longrightarrow O^+(4S) + N(4S)$	$\gamma_{28} = 5.0 \times 10^{-19}$	
$N^+ + H \longrightarrow H^+ + N(4S)$	$\gamma_{29} = 3.6 \times 10^{-18}$	
$N^+ + O_2 \longrightarrow O_2^+ + N(2D)$	$\gamma_{33} = 2.0 \times 10^{-16}$	

Tab. 2.1: Chemical reactions in the E-region and reaction rates.

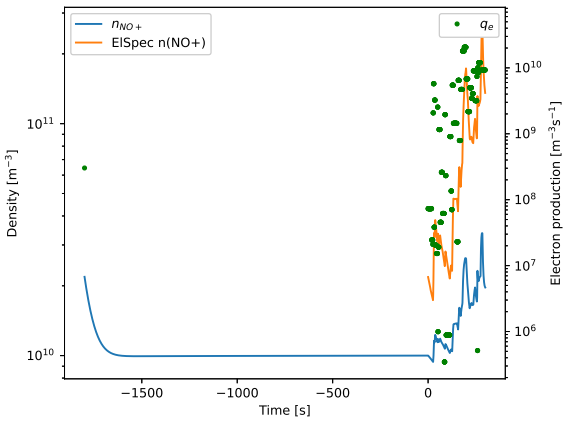

Fig. 2.1: The density of NO^+ at 96 km altitude is shown. During the first 30 minutes, the model ionosphere is allowed to find an equilibrium state. Orange shows the assumed NO^+ density for ElSpec, corrected for charge neutrality. Blue shows the first iteration of the ionospheric chemistry model.

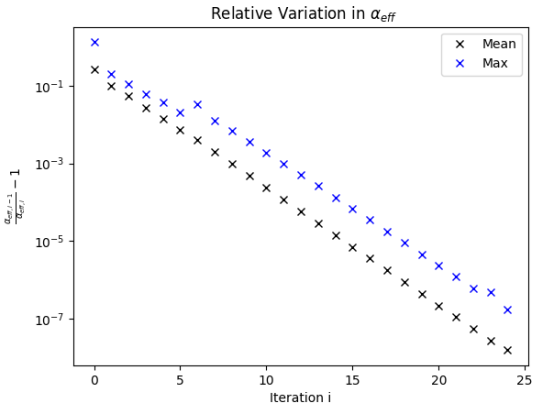

Fig. 3.1: The mean and maximum values of relative deviation of the effective recombination rate over iterations ($(\alpha_{i-1} - \alpha_i)/\alpha_i$) show that the effective recombination rate indeed converges.

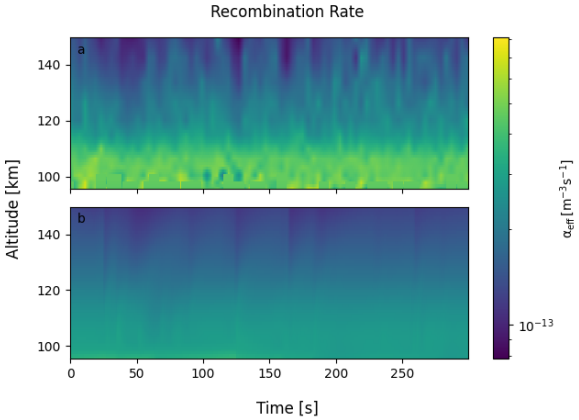

Fig. 3.2: The effective recombination rate is shown for (a) the first iteration of ElSpec, and (b) the last iteration of Ion Chemistry.

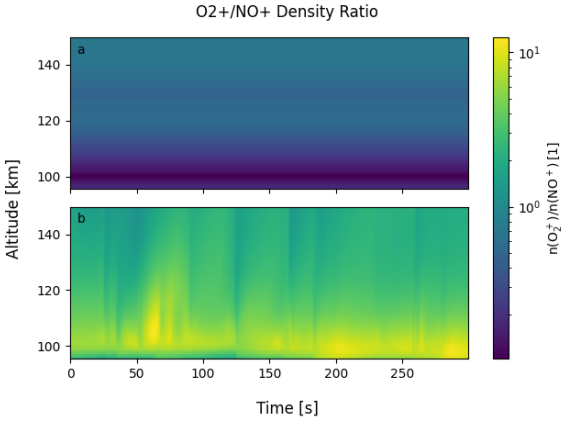

Fig. 3.3: The ratio of O_2^+/NO^+ is shown for (a) the first iteration of ElSpec and (b) the last iteration of Ion Chemistry.

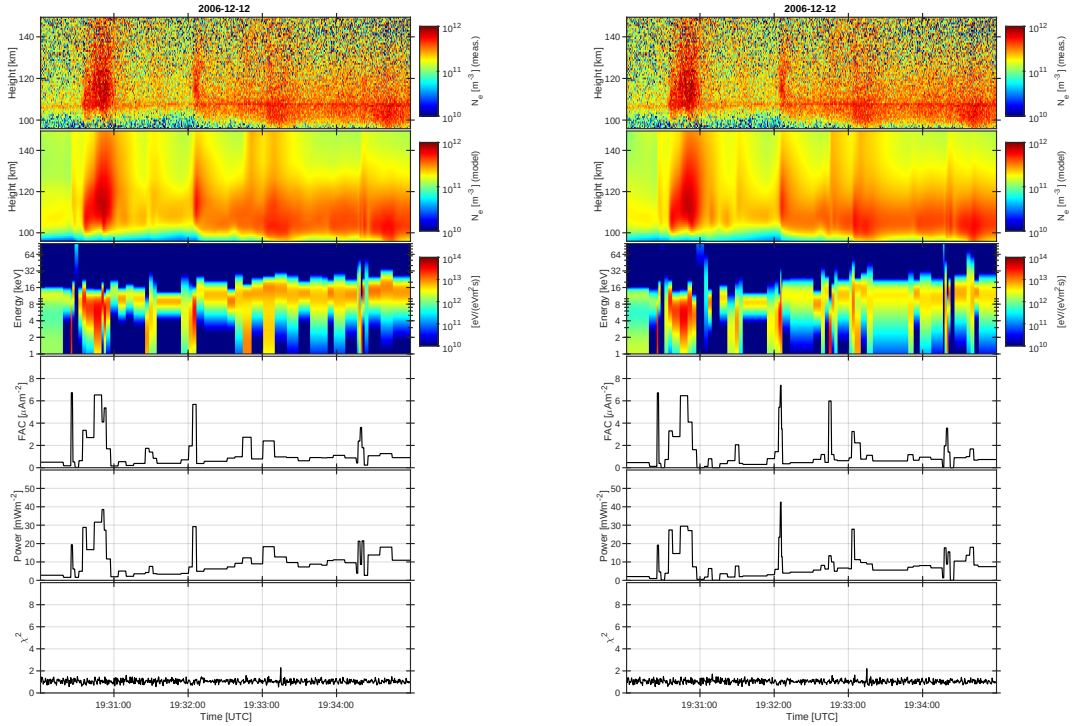

a b

Fig. 3.4: ElSpec results with (a) constant ionospheric densities and (b) variable ionospheric densities.

References

[1] Dieter Bilitza et al. "The International Reference Ionosphere 2012 – a model of international collaboration". en. In: *Journal of Space Weather and Space Climate* 4 (2014). Publisher: EDP Sciences, A07. ISSN: 2115-7251. DOI: 10.1051/swsc/2014004. URL: https://www.swsc-journal.org/articles/swsc/abs/2014/01/swsc130043/swsc130043.html (visited on 03/06/2023).

[2] Xiaohua Fang et al. "Parameterization of monoenergetic electron impact ionization". en. In: *Geophysical Research Letters* 37.22 (2010). _eprint: https://onlinelibrary.wiley.com/doi/pdf/10.1029/2010GL045406. ISSN: 1944-8007. DOI: 10.1029/2010GL045406. URL: https://onlinelibrary.wiley.com/doi/abs/10.1029/2010GL045406 (visited on 05/30/2022).

[3] R. A. Jones and M. H. Rees. "Time dependent studies of the aurora—I. Ion density and composition". en. In: *Planetary and Space Science* 21.4 (Apr. 1973), pp. 537–557. ISSN: 0032-0633. DOI: 10.1016/0032-0633(73)90069-X. URL: https://www.sciencedirect.com/science/article/pii/003206337390069X (visited on 09/22/2022).

[4] M. H. Rees. *Physics and Chemistry of the Upper Atmosphere*. Cambridge Atmospheric and Space Science Series. Cambridge: Cambridge University Press, 1989. ISBN: 978-0-521-36848-3. DOI: 10.1017/CBO9780511573118. URL: https://www.cambridge.org/core/books/physics-and-chemistry-of-the-upper-atmosphere/B92A6E9E87492A19A407C4681E674EA6 (visited on 06/08/2022).

[5] Joshua Semeter and Farzad Kamalabadi. "Determination of primary electron spectra from incoherent scatter radar measurements of the auroral E region". en. In: *Radio Science* 40.2 (2005). _eprint: https://onlinelibrary.wiley.com/doi/pdf/10.1029/2004RS003042. ISSN: 1944-799X. DOI: 10.1029/2004RS003042. URL: https://onlinelibrary.wiley.com/doi/abs/10.1029/2004RS003042 (visited on 05/02/2022).

[6] Ilkka I. Virtanen et al. "Electron Energy Spectrum and Auroral Power Estimation From Incoherent Scatter Radar Measurements". en. In: *Journal of Geophysical Research: Space Physics* 123.8 (2018). _eprint: https://onlinelibrary.wiley.com/doi/pdf/10.1029/2018JA025636, pp. 6865–6887. ISSN: 2169-9402. DOI: 10.1029/2018JA025636. URL: https://onlinelibrary.wiley.com/doi/abs/10.1029/2018JA025636 (visited on 04/21/2022).